Pergamon

Geochimica et Cosmochimica Acta, Vol. 67, No. 1, pp. 75–83, 2003

0016-7037/03 $22.00 + .00

PII S0016-7037(02)01041-4

XANES mapping of organic sulfate in three scleractinian coral skeletons

JEAN-PIERRE CUIF,[1,*] YANNICKE DAUPHIN,[1] JEAN DOUCET,[2] MURIELLE SALOME,[2] and JEAN SUSINI[2]

[1]Université Paris XI, Géologie, Bat. 504, Orsay 91405, France (FRE2566 Orsay-Terre)
[2]European Synchrotron Radiation Facility, Grenoble, France

(*Received December* 3, 2001; *accepted in revised form July* 1, 2002)

Abstract—The presence and localization of organic sulfate within coral skeletons are studied by using X-ray absorption near edge structure spectroscopy (XANES) fluorescence. XANES spectra are recorded from four reference sulfur-bearing organic molecules: three amino acids (H-S-C bonds in cysteine; C-S-C bonds in methionine; one disulfide bond C-S-S-C bonds in cystine) and a sulfated sugar (C-SO_4 bonds in chondroitin sulfate). Spectral responses of three coral skeletons show that the sulfated form is extremely dominant in coral aragonite, and practically exclusive within both centres of calcification and the surrounding fibrous tissues of coral septa. Mapping of S-sulfate concentrations in centres and fibres gives us direct evidence of high concentration of organic sulfate in centres of calcification. Additionally, a banding pattern of S-sulfate is visible in fibrous part of the coral septa, evidencing a biochemical zonation that corresponds to the step-by-step growth of fibres.

1. INTRODUCTION

A reliable scheme for fine-scale structure and composition of coral skeletons is a key point in sedimentological and paleoenvironmental research as in taxonomic and evolutionary studies. Despite a long-standing recognition of the aragonitic mineralogy of scleractinian corallites, a model of coral skeletons is not yet generally agreed. More precisely, different opinions still exist on the level at which chemical relationships (if any) are established between mineral and organic materials during the biomineralization process.

The fibrous organization of aragonite in coral skeletons was first observed by Pratz (1882). Emphasizing similarities between spherulitic crystallization that occur in saturated solutions and the fibrous fan-systems frequently observed in microscopic studies of coral skeletons, Bryan and Hill (1941) developed the concept of coral fibre as "a single orthorhombic crystal of aragonite." Most of the sedimentological studies dealing with diagenetic process and isotopic or trace element measurements aiming to reconstitute ancient environments are still based on this concept of a pure mineral coral fibre.

However, Goreau (1959), Mitterer (1978), Johnston (1980), and Constantz and Weiner (1988) progressively show that specifically secreted organic components are involved in the process of coral fibre crystallization. Johnston (1980) pointed out that "attempts to implicate these organic materials in the processes that control and direct mineralization have largely been made in ignorance of this material's spatial distribution and microarchitecture within the skeleton" (p. 178).

The first aim of the present paper is to present chemical evidence of the localization of organic compounds within coral fibres, in accordance with the stepping growth process that was previously evidenced (Cuif and Dauphin, 1998).

Coral skeletons are not built only by fibres. Centres of calcification, "the point from which fibres diverge" (Ogilvie, 1896), have been characterized by gathering scanning electron microscope (SEM) observations, Raman spectrometry, electron microprobe measurements of minor elements (Cuif and Dauphin, 1998), ultraviolet (UV) autofluorescence and fluorochrome staining (Gautret et al., 2000). Sulfur microprobe measurements have allowed the differences between centres of calcification and fibres to be evidenced. Electrophoretic studies of biochemical compounds extracted from coral skeletons and in situ histochemical characterization have drawn attention to the presence of organic sulfate in coral skeletons (Dauphin and Cuif, 1997; Dauphin, 2001).

Thus, the question arises of the possible correspondence between the S detected by electron microprobe measurements (Bar-Matthews et al., 1993) and S as an element of sulfated sugars in biochemically studied coral skeleton mineralizing matrices. Taking advantage of the high quality X-ray beams available at the European Synchrotron Radiation Facility (ESRF) at Grenoble, France, we report here a mapping experiment focussing on S chemical status and localization in the septa of scleractinian corals.

2. MATERIAL AND METHODS

2.1. Checking Specimens and Preparing the Coral Structures

Recently collected coral specimens were used. They belong to species living in very different areas. *Montastrea curta* and *Favia stelligera* are zooxanthellate corals from Polynesia (Mururoa and Moorea islands respectively). On the other hand, *Lophelia pertusa* is a deep-sea coral from the northeast Atlantic continental slope. The analyzed specimen was dredged near the Azores islands (CENTOB collection, in Brest, France), at 850 m depth. After removal of polyp tissues by using dilute sodium hypochlorite, quality of skeletons was first studied by SEM. Polished surfaces are prepared and exposed during 40 s to a solution of 0.1% formic acid in Milli-Q water, 3% glutaraldehyde. This allows the differences between microstructural patterns of centres of calcification and fibres to be exposed and the absence of endolithic borers to be assessed. This method is used to examine the polished surfaces after X-ray absorption near edge structure spectroscopy (XANES) mapping has been carried out, and to check the correspondence between S repartition and septal microstructures.

Sections of septa to be analysed by XANES were selected by examination of polished surfaces (prepared in the quality-checked specimens) under a UV epifluorescence microscope. This observation

* Author to whom correspondence should be addressed (cuif@geophy.geol.u-psud.fr).

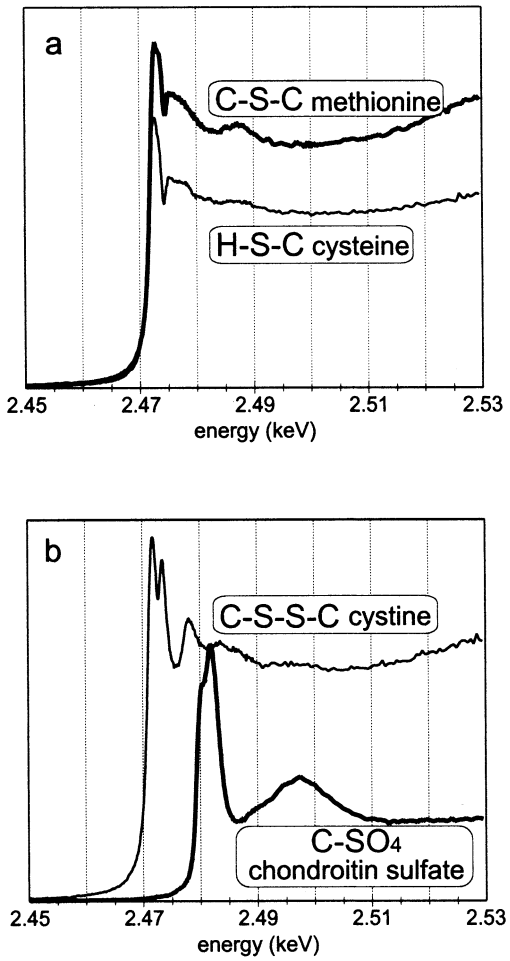

Fig. 1. Reference XANES spectra for four sulfur-bearing pure molecules. The three spectra given by amino acids are clearly distinct from the spectrum of the highly oxidized sulfur in chondroitin sulfate, from both global profile and peak position.

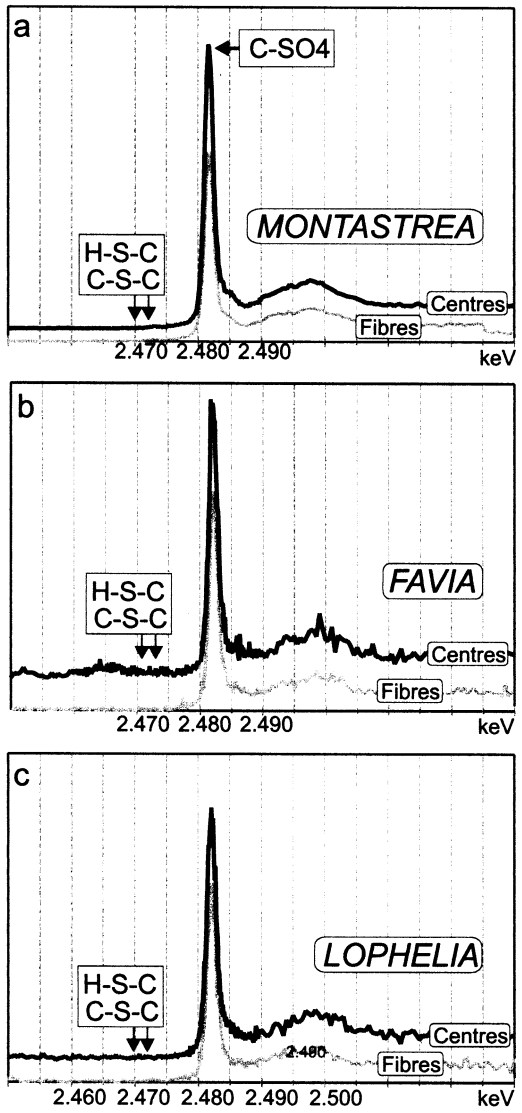

Fig. 2. Localized XANES spectra in centres of calcification and surrounding fibres on the polished surfaces of *Montastrea* (a), *Favia* (b), and *Lophelia* (c). No signal is given in the energy domains that correspond to S-amino acids (2.47 keV), whereas an intense response is obtained at the energy of sulfated glucids (2.48 keV).

allows the position of the early mineralization zone (EMZ) (i.e., the trace of the distal growth edge within the septum) to be recognized. When mounting the specimens onto the object-holder of the ID-21 X-ray microscope, attention was paid to include both centres and fibrous components of coral septa in the 100 $\times$ 100 μm zones to be mapped.

2.2. Sulfate Mapping

Molecular environment of a given atom can be characterized by tuning the energy of the probing X-rays photons close to the absorption edge of the element. At the ID-21 line a high-resolution, fixed-exit, double crystal Si111 monochromator allows very precise selection of used energies to be obtained, resulting in distinguishable spectra for the different coordination status of sulfur. To increase analysis resolution, a Fresnel zone plate acting as focussing optics generates an X-ray probe of a submicronic diameter.

Preexperiment checking of spectral accuracy has been carried out by using pure molecules containing sulfur with various bonds. Reference spectra were established for disulfide bonds (C-S-S-C) in cystine, H-S-C bonds in cysteine, C-S-C in methionine, and C-SO_4 in chondroitin sulfate (Fig. 1a,b).

In a first step of specimen characterization, localized spectra for S coordination in coral skeletons are collected from centres of calcification and fibres, on a wavelength interval corresponding to references obtained from the pure chemical molecules (Fig. 2). This first step is followed by mapping itself. A 100 $\times$ 100 μm field on the mounted specimen (Figs. 3a, 4b) can be point-by-point analysed, a piezoelectric device providing high-precision positioning in both vertical and horizontal stepping. To minimize the effect of elastic scattering on the collected signal, the surface specimen is 15° tilted with respect to the beam direction. The energy-dispersive Ge-detector (Princeton-Gamma-Tech) is mounted in the horizontal plan to collect the fluorescence emission photons. In our examples, sulfate bonds were mapped by using an energy of 2.482 keV, just beyond the sulfur K edge, and corresponding to the energy position of the XANES peak. The dwell time was fixed to 1 s. The 50-nm-diameter X-ray beam allows high mapping resolution to be reached: 0.50 to 0.70 μm, depending on size of the mapped sector.

After mapping, the polished surface is slightly etched (as in the preparative step), to evaluate the significance of localized differences with respect to the microstructures of the mapped surfaces.

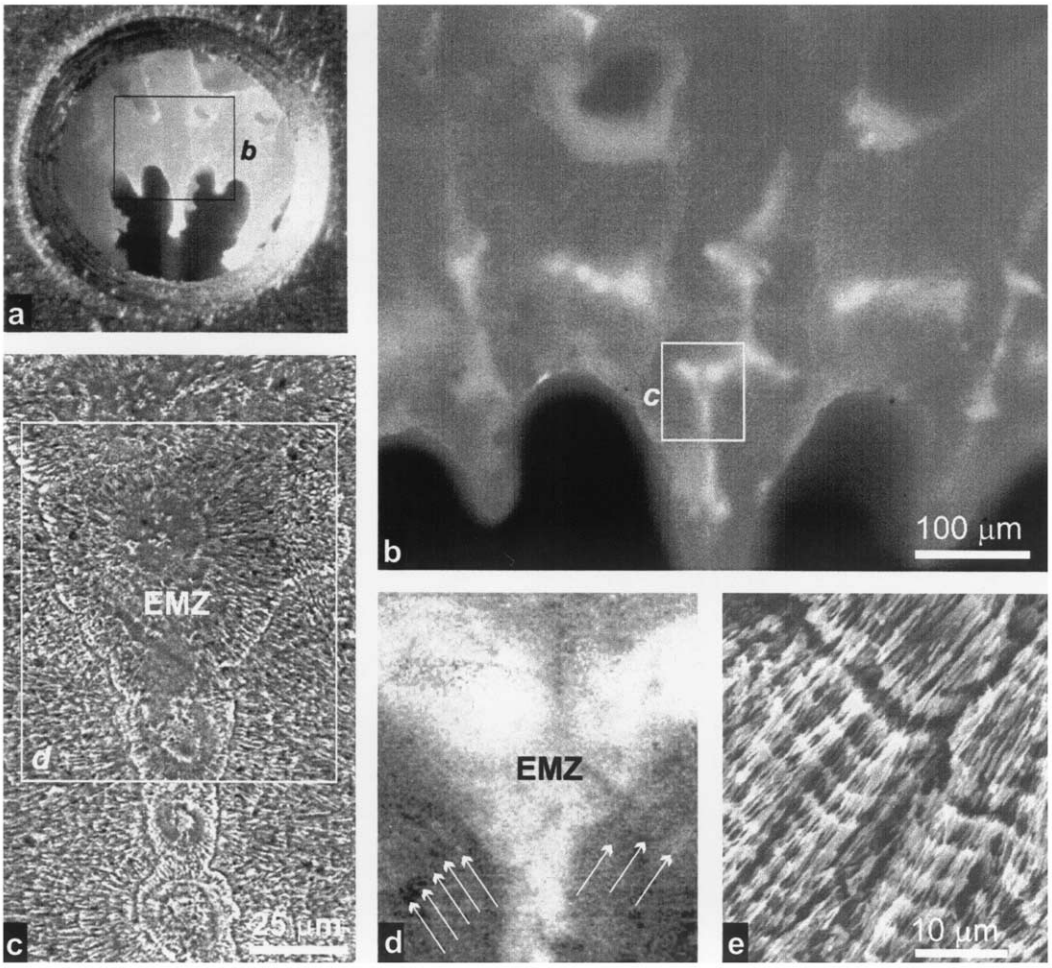

Fig. 3. *Montastrea curta*. (a) Polished surface in a corallite in the object holder of XANES microscope, showing the mapped zone. Hole diameter: 1.5 mm. (b) UV autofluorescence of the same surface; note the strong fluorescence in the centres of calcification (EMZ). (c) Microstructural patterns of the mapped zone (white frame); note the visible difference of microstructural pattern between the EMZ and the fibrous layers. (d) XANES map showing the repartition of S-sulfate. Note the high concentration in the centres of calcification (EMZ) and the banding pattern in fibres (arrows), visible although S concentrations are weaker. Horizontal field: 70 μm. (e) Polished and etched surface showing the banding growth pattern of fibres (SEM).

2.3. Technical Information Concerning Data Used in Discussion (Raman Spectrometry, Infrared Spectrometry, Electrophoresis, Thermogravimetry)

2.3.1. Raman Spectrometry

Measurements were made at the LASIR-CNRS laboratory at Thiais, France. Raman spectra were recorded at room temperature with a XY Dilor spectrometer LZ2 cooled charge-coupled device detector. Operative conditions were: excitation by red laser beam 514.5 nm, laser power at sample 4 mW, grating 1800, slit width 150 μm, integration time 3 min 30 s. Raman spectra were obtained on the range 570 to 1400 cm^{-1}.

2.3.2. Extraction and Purification of Skeletal Organic Matrices

Before decalcification, possible minute remains of polyp tissues were dissolved in NaClO, corallites were rinsed with Milli-Q water, room temperature dried, and grounded into calibrated powders to ensure regularity of the decalcifying process. A 3-g standard aliquot of corallite powder is immersed into 25 mL Milli-Q water. Under continuous stirring, decalcification is done by adding acetic acid (Normapure grade), under permanent pH control by Radiometer titrator (pH fixed to 4). A centrifugation (3 500 *g* for 15 min) allows supernatant (soluble) and precipitated (insoluble) fractions to be separated. Soluble fractions are desalted by using a Filtron ultrafiltration cell (3 kDa cut-off membrane) against Milli-Q water, followed by concentration and lyophilization.

2.3.3. Infrared Spectrometry

All spectra were recorded at 4 cm^{-1} resolution with 64 scans (measurement time: 4.2 min) with a strong Norton-Beer apodization on a Perkin-Elmer model 1600 Fourier transform infrared spectrometer (FTIR), in the wave-number range 4000 to 450 cm^{-1}. Thus, the spectrometer was equipped with a diffuse reflectance accessory, which permits diffuse reflectance infrared Fourier transform (DRIFT) measurements with high sensitivity on powders. All spectra were corrected by the Kubelka-Munk function. The system was purged and permanently maintained under nitrogen to reduce the atmospheric CO_2 and H_2O absorption. Before a spectrum was run, the height of the sample

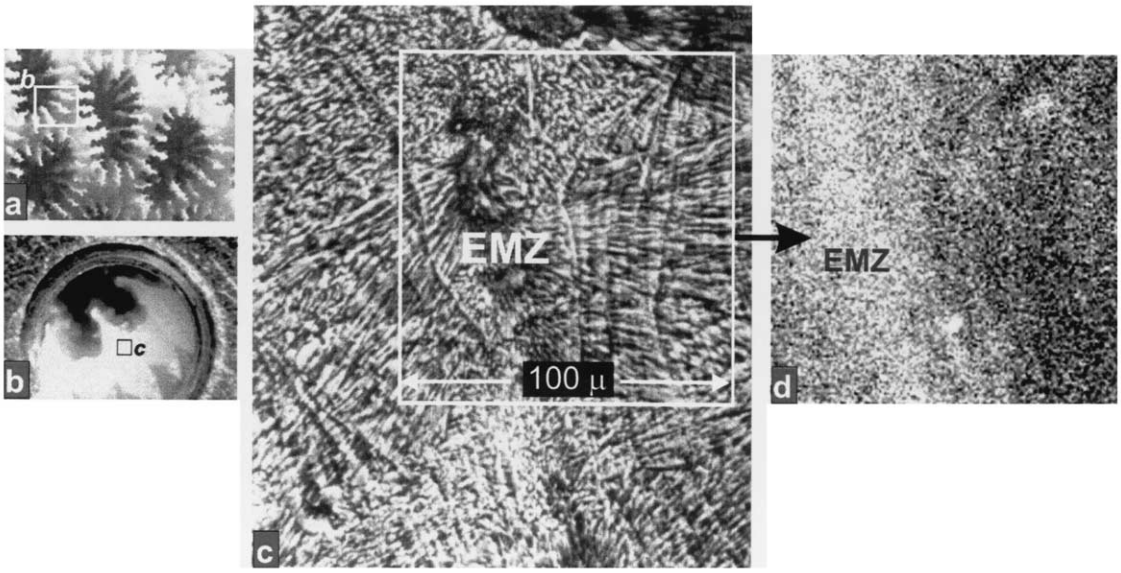

Fig. 4. *Favia stelligera*. (a) Global view of corallites (mean size: 3 to 6 mm). (b) Polished surface in a corallite in the object holder of XANES microscope, showing the mapped zone. Hole diameter: 1.5 mm. Frame: mapped zone on the polished surface. (c) Microstructure of the mapped zone (white frame) after the postmapping etching (SEM). Banding growth pattern of fibre is well visible. (d) XANES mapping of the S-sulfate showing the high S-concentration in the zone of centres of calcification (EMZ). Horizontal field: 100 μm.

cup was adjusted by using the alignment routine provided by Perkin-Elmer, so that a maximal signal throughput was obtained. A background spectrum was measured for pure KBr. Sample spectra were automatically ratioed against background to minimize CO_2 and H_2O bands. All samples and KBr were reduced to a powder by grinding with an electric mortar to obtain homogeneous granulometry. They were dried in an oven at 38°C overnight. Powdered samples and KBr were mixed (~5% powdered samples in KBr).

2.3.4. Isoelectric Focalization of Organic Soluble Compounds

Isoelectric points were determined according to Dauphin and Cuif (1997, 1999). One-dimensional microslab isoelectric focussing (IEF) was done in homogeneous polyacrylamide small gels (5%T, 3%C), 5% carrier ampholytes Bio-Lyte (Bio-Rad) pH 3 to 10, 25% glycerol. With the Bio-Rad Model 111 Mini-IEF cell, the gel was run without electrode buffers: nondenaturing dry IEF. The lyophilized matrices were redissolved in Milli-Q H_2O. Focussing was carried out in a stepped fashion to prevent overheating: 15 min at 100 V, 15 min at 200 V, and ~50 min at 450 V.

Two staining procedures were used: acridine orange and alcian blue. For both methods, gels were placed in a solution of methanol (40%) and acetic acid (10%) for 30 min (fixing solution). Acridine orange was dissolved in Milli-Q H_2O (20 mg acridine–95 mL H_2O–5 mL methanol). Gels were placed in the solution for 30 min, then destained with Milli-Q H_2O. The staining solution was made of 0.5% alcian blue GX in 3% acetic acid. The destaining solution contained 25% ethanol and 7% acetic acid.

Markers were as follows: bovine serum albumin (BSA) and chymotrypsin were stained with Coomassie blue R250. Several isoelectric points (pI) are known for BSA, 4.9 and 5.2 being the most frequently described. Chymotrypsin shows two main pI (9 and 9.1).

2.3.5. Thermogravimetric Measurements

Thermogravimetric measurements were made at the University Paris-XI laboratory, Physico-Chimie des Matériaux. Calibrated powders were prepared from carefully cleaned and dried coral skeletons. Weight loss during heating was recorded on a SETARAM TG-DTA92, between room temperature and 450°C.

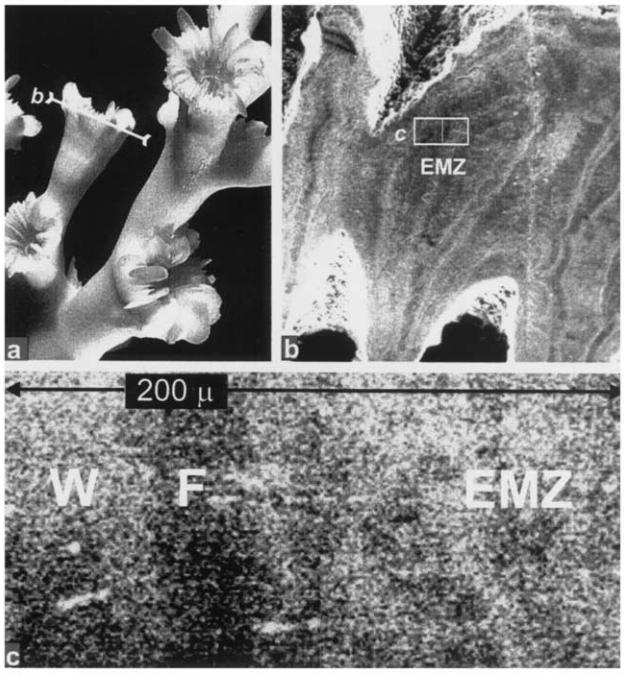

Fig. 5. *Lophelia pertusa*. (a) Corallites. Mean diameter of branches: 7 mm. (b) Position of the mapped zone on the polished surface prepared near the corallite upper part (SEM). (c) XANES mapping of the S-sulfate showing the high S-concentration in the zone of centres of calcification (EMZ). W: wall, F: fibres.

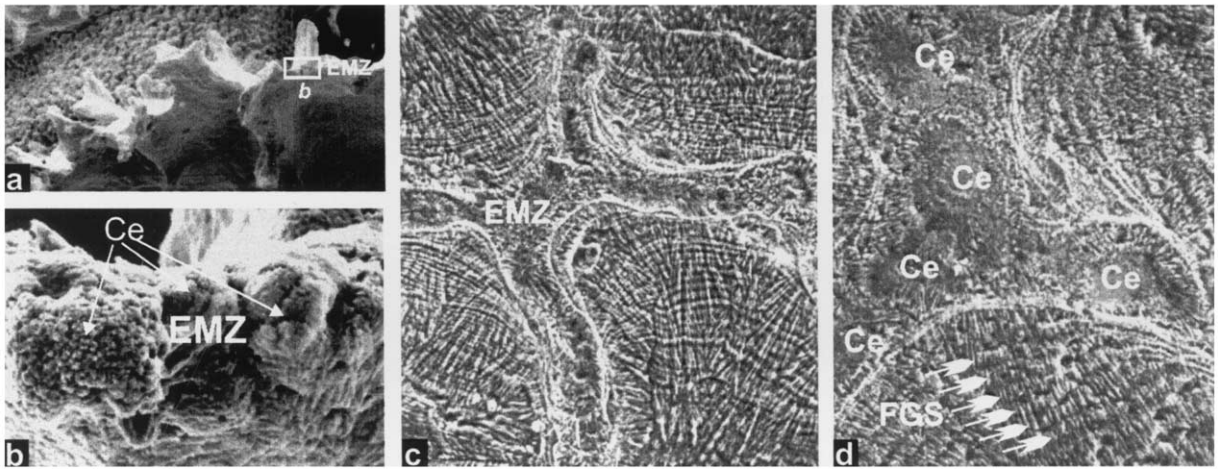

Fig. 6. Morphologic and microstructural relationships between centres of calcification and fibres in *Favia stelligera* (SEM). (a) Upper view of a growing edge of a septum (see also Fig. 4a). Horizontal field: 1 mm. (b) Detailed view of the growing edge. Patches of microgranular aragonite (Ce = centres of calcification) exemplify the microstructural specificity of the EMZ. Horizontal field: 50 μm. (c) Polished and etched section prepared a few millimeters below the growing edge of septa. The EMZ is clearly visible, as well as the stepping growth process of fibres. Horizontal field: 200 μm. (d) Detailed view showing contiguous patches of microcrystalline aragonite in centres of calcification (Ce) and the stepping growth process of fibres (FGS = fibre growth steps). Horizontal field: 70 μm.

3. RESULTS

3.1. XANES Spectrum in Centres and Fibres

In all cases, sulfated compounds were detected in both centres of calcification and fibres (Fig. 2). A precise correspondence of the maximum energy peak with previously recorded S-bond in chondroitin sulfate is observed, and global patterns of spectra from coral skeletons are in excellent correspondence with the spectrum obtained from the sulfated glucidic reference (chondroitin sulfate).

In contrast, the energy domains corresponding to S-bearing amino acids do not show visible signals. In skeletal matrix proteins, the S content (if any) remains always insignificant compared with the S from sulfated sugars.

3.2. Sulfate XANES Maps

All analyzed fields show localized differences with respect to the S-sulfate concentrations. Taking into account the size of the mapped squares (100 $\times$ 100 μm), only a part of the septal surface can be studied in each case. Additionally, as septal microstructures (i.e., the spatial arrangements of centres of

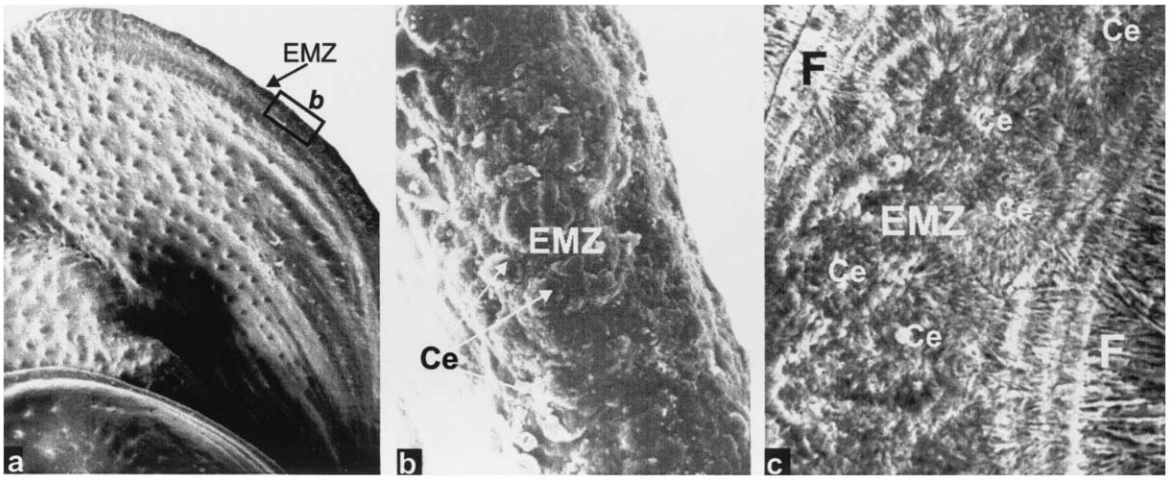

Fig. 7. Centres of calcification in *Lophelia pertusa* (SEM; see also Fig. 5a). (a) Oblique view of a septum. Horizontal field: 2.5 mm. (EMZ = early mineralization zone). (b) Detailed view of the EMZ. Patches made by centres of calcification are also well visible. In this species, centres of calcification (Ce) generally built a thick and continuous structure at the growing edge of septa. Horizontal field: 100 μm. (c) Polished and etched section focussing on the first growth steps of fibres (F), in contact to the sides of the EMZ (Ce = centres of calcification). Horizontal field: 75 μm.

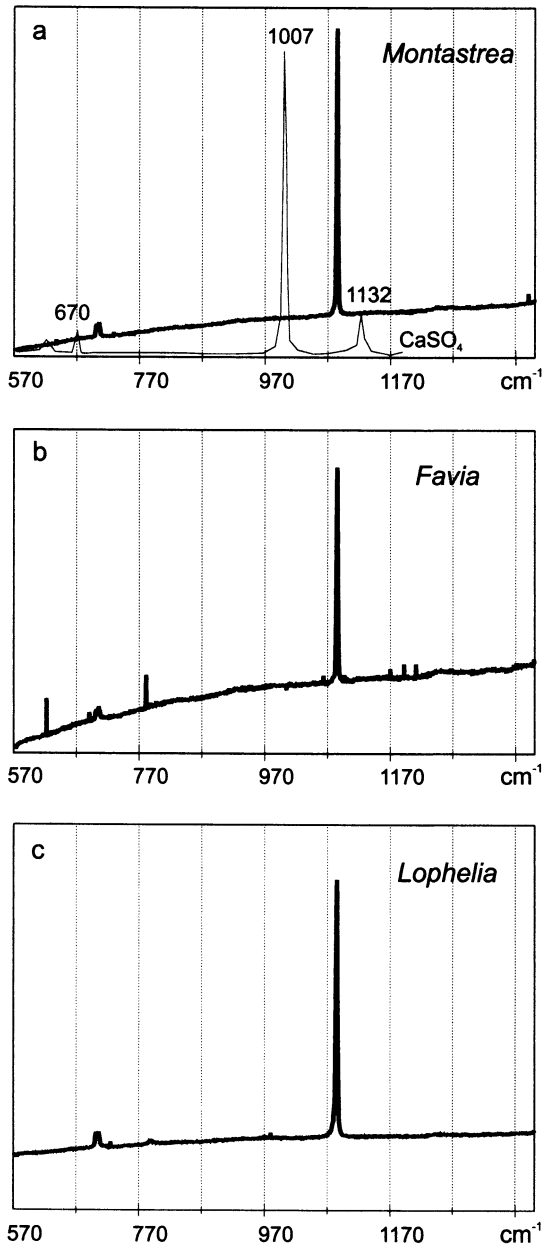

Fig. 8. Raman spectra showing the absence of $CaSO_4$ and the presence of the major band of aragonite in the three studied species.

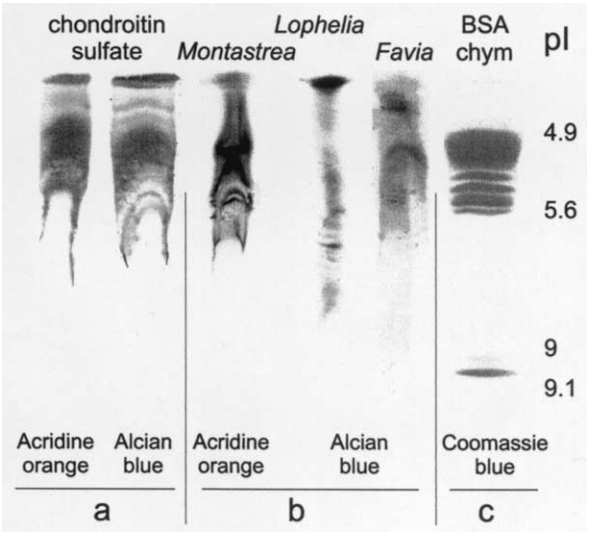

Fig. 9. Isoelectric focalization electrophoresis and specific staining for: (a) chondroitin sulfate (acidic sugar), stained by acridine orange and alcian blue; (b) soluble organic matrices isolated from skeletons of the three studied species; (c) reference proteins, BSA and chymotrypsin (pI: isoelectric point). Standard proteins are not stained by acridine orange and alcian blue.

calcification and fibres) are different, depending on taxonomic position of the species, results cannot be read without positioning the selected areas in the septa.

3.2.1. *Montastrea curta*

A strong contrast exists between concentrations of S-sulfate in the EMZ ("centres of calcification") and the surrounding fibres (Fig. 3d). In this species, UV fluorescence of the EMZ is also intense (Fig. 3b), a property that helped to select the zone to be mapped. XANES mapping of S-sulfate demonstrates an exact correspondence between the high UV fluorescence localization (Fig. 3b), the high S-sulfate concentrations (Fig. 3d), and the EMZ that is globally in the median part of the septa (Fig. 3c).

A global drop of S-sulfate concentration occurs in the fibrous zone, on both sides of the EMZ. A banding pattern of the S-sulfate in fibres is also visible (Fig. 3d, arrows) that corresponds to the early steps of fibre growth.

3.2.2. *Favia stelligera*

Auto-fluorescence of the EMZ is weak, compared with the high response of *Montastrea*. However, sulfate mapping makes also visible the difference between the EMZ and the fibrous part of the septa (Fig. 4c, d). The high concentration zone (Fig. 4d) corresponds to the line of centres of calcification (some of them being visible on the postmapping SEM observation: Fig. 4c). Laterally, although only one side of the fibrous development is visible, due to the size of analyzed field, the drop in sulfate concentration is also visible, whereas a weak banding pattern appears, that corresponds to the successive growth step of the fibrous zone (Fig. 4c).

3.2.3. *Lophelia*

The mapped zone was at the contact between septa and the first deposition of the corallite wall (Fig. 5b). Taking into

Table 1. Sulfur concentrations (ppm) in the early mineralization zones ("centres of calcification") and in surrounding fibres for the three studied species.

	Montastrea	Favia	Lophelia
Centres	3570	2510	1720
Fibres	1700	1700	1260
Difference	1870	810	460

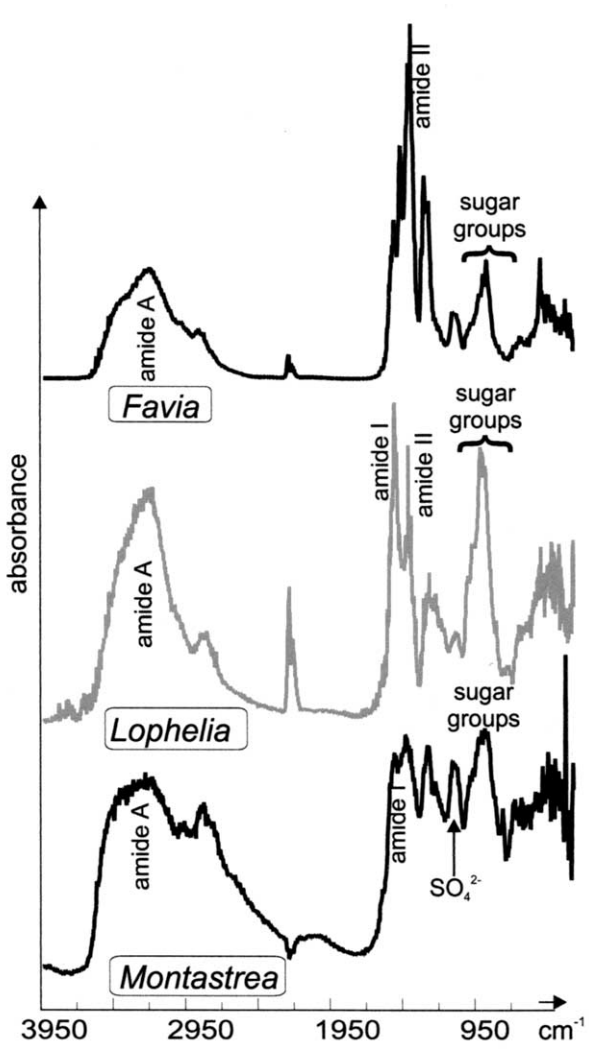

Fig. 10. Infrared profiles for the isolated soluble matrices of calcareous skeletons. Note the diversity in global response on the amide A domain between 3700 and 3250 cm^{-1}. In the specific domain of sugars, the SO_4^{2-} band is well developed in *Montastrea* and weaker in *Lophelia* and *Favia*.

account the microstructural organization of skeletal components in *Lophelia*, we have made two adjacent 100 × 100 μm maps. Thus, the picture is a little bit more complex. It includes the EMZ of the major septa (Fig. 5c: EMZ) that shows high but diffuse sulfate concentration, a zone with lower sulfate concentration in the fibrous part of the septa (Fig. 5c: F), and laterally a part of the corallite wall (Fig. 5c: W). In *Lophelia*, the corallite wall is built by an independent structure, with its own early calcification zone that also shows a higher S-sulfate level.

4. DISCUSSION

As Johnston (1980) pointed out, "no reliable model of growth process can be proposed since analytical data cannot be correlated to structural observations carried out at relevant scale." Comparison of SEM microstructural pictures and XANES mapping indicates a difference in organic S content between centres of calcification and fibres, which clearly corresponds to micromorphological patterns of skeletal components.

4.1. Microstructural Patterns in Centres of Calcification and Fibres

The specific crystallization patterns of aragonite in the EMZ of corals is well evidenced here, by specific etchings in *Favia* (Fig. 6) and *Lophelia* (Fig. 7). These pictures show the differences between crystallization patterns in centres and fibres on a wider scale than the restricted zone mapped in Figures 4 and 5.

XANES results emphasize the biologic peculiarity of centres of calcification during the coral skeleton growth process. These 10- to 40-μm round-shaped domains, variously arranged from species to species, are the first points where calcification occurs at the upper parts of septa. Observation by Gladfelter (1982) of "randomly oriented fusiform crystals" at the growing tips of *Acropora* skeletons was tentatively extended to all coral species, and further observations fully support this hypothesis (Cuif and Dauphin, 1998). Nevertheless, the possible involvement of an organic matrix in the formation of the two-phased construction of *Acropora* skeleton was considered as "not yet ascertained" by Gladfelter. Results of XANES mapping allow the precise correspondence between concentrations of acidic sulfated polysaccharides and microstructural patterns of the EMZ to be established.

The long-standing observation that these parts of coral skeletons always appear very sensitive to diagenetic alteration even in recent corals (Sorauf, 1972, 1980; Sorauf and Cuif, 2001) can be explained by their higher concentration of organic compounds.

4.2. Organic or Mineral Sulfate

Microprobe measurements by Bar-Matthews et al. (1993) indicate SO_3 concentration between 3740 and 4400 ppm. Localized measurements in centres of calcification and fibrous skeletons for the three species studies here (Cuif and Dauphin, 1998) gave the following results (S concentrations). They are globally in agreement with the Bar-Matthews data, but showed a chemical difference between centres and fibres.

4.2.1. Localized Raman Spectrometric Data

Localized Raman spectrometry on both centres of calcification and fibres in the presently studied species show no indication of mineral sulfate (Fig. 8): the major bands for gypsum (1008 cm^{-1} and 1137 cm^{-1}) or anhydrite (1017 cm^{-1}, 1129 cm^{-1}, and 1160 cm^{-1}) are absent. The main band observed in the three samples at 1084 cm^{-1} shows the presence of carbonate, and confirms previous results showing the aragonitic composition of both centres and fibres (Cuif and Dauphin, 1998). Consequently, the whole sulfate content is in the organic skeletal matrix.

4.2.2. Thermogravimetric Measurements

This result suggests an inconsistency between the high organic sulfur concentration and the low values of intraskeletal organic matrix that are commonly admitted (0.2 to 0.3%). However, thermogravimetric measurements of weight loss between ambient and 450°C suggest that the proportion of non-

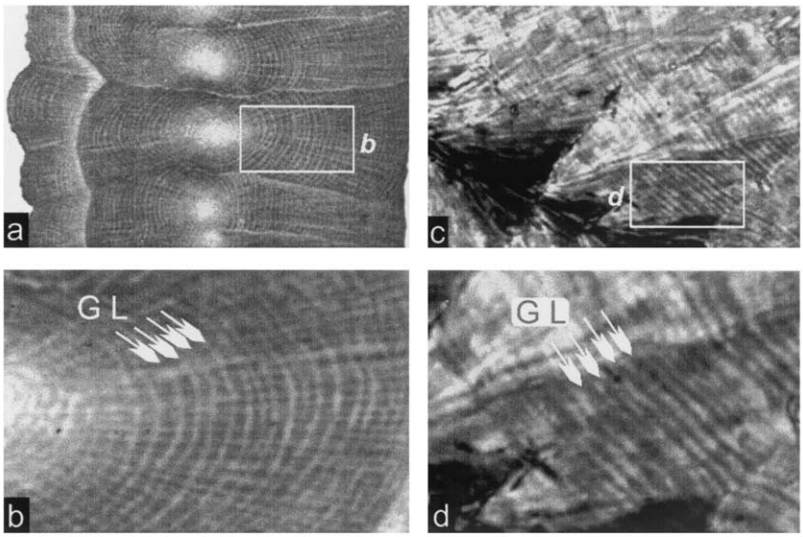

Fig. 11. The stepping growth process in coral fibres.(a) Original picture by Ogilvie (1896), focussing on centres of calcification. (b) Enlargement of the picture: the growth lines (GL) are clearly visible. (c) Coral fibres observed in polarized light. On very thin sections (~8 to 10 μm thick), the growth lines may be visible. Horizontal field: 170 μm. (d) Detail of (c). The growth step scale corresponds to dimensions observed in both SEM observations and XANES mapping. GL: growth lines. Horizontal field: 50 μm.

mineral components of coral skeletons should be higher. In four species similar values have been observed: *Porites* 2.45%, *Favia* 2.52%, *Montastrea* 2.55%, and *Lophelia* 2.75%. It is known (Gaffey, 1988) that water is present in calcareous invertebrate skeletons. Presently, the ratio of organic molecules and linked water cannot be assessed, but percentages of skeletal organic components higher than 0.3% are probable.

4.2.3. Electrophoretic and DRIFT Data

Presence of organic sulfur in coral skeletons was confirmed in numerous species by IEF electrophoresis of isolated skeletal organic components (Dauphin and Cuif, 1997). Various molecular patterns are shown in skeletal matrices stained by alcian blue and acridine orange, two specific dyes for sulfated acidic sugars (chondroitin sulfate). In contrast, they do not stain standard proteins such as BSA or chymotrypsin (Fig. 9, right column).

Studies of isolated matrices by two-dimensional electrophoresis and infrared absorption (Dauphin, 2001) provide us with consistent results concerning methods by which the quantity of sugars in organic matrices can be estimated. The three species studied here exemplify this result, allowing a good correspondence between S contents (Table 1) and absorbance areas in the sugar group wavelength domains to be noticed (Fig. 10). Moreover, the SO_4 band is stronger in *Montastrea* than in *Lophelia*, the weakest one being observed in *Favia*.

Thus, before the reported XANES mapping experiment, it was established (but without localization) that sulfated acidic polysaccharides could be the origin of S content in coral skeletons, whereas it was also known (but without chemical information) that S as a chemical element was more abundant in centres of calcification than in the fibrous part of the same skeletons.

On this basis, pictures of global repartition of S-sulfated bonds obtained by XANES mapping give decisive documents. Higher concentrations of S in centres of calcification that built the EMZ can be unequivocally related to differences in concentration of the sulfated polysaccharides between centres of calcification and fibres.

4.3. Growth Pattern of Fibres

Attention should be paid to repartition patterns of sulfated acidic polysaccharides. In *Montastrea*, for instance, the banding pattern of sulfate (Fig. 3d, arrows) corresponds to the structural growth steps shown by an etched surface (Fig. 3e). To date, this picture gives us the most direct evidence of the cyclic secretion of mineralizing matrices (here illustrated by its sulfated component), in close correlation with the growth steps of the aragonitic fibrous units.

In contrast to a purely chemical crystallization of aragonite in coral fibres, a concept still widely admitted in research dealing with coral as paleoenvironmental records, data collected in this work support a biochemically driven crystallization process ("matrix mediated mineralization," Lowenstam, 1981).

Very thin sections made in fibrous fascicles that built coral skeletons sometimes allow the banding pattern to be clearly observed (Fig. 11c,d). Due to the high sulfate content of coral skeleton mineralizing matrices, the XANES mapping allows the matrix cyclic repartition to be correlated to fibre growth steps.

5. CONCLUSION

XANES mapping allows the localization of the sulfated glucidic components of coral skeletons to be localized. High concentrations are present in EMZ (the "centres of calcification"). In fibres, sulfated compound concentrations are weaker,

but a banding pattern is visible corresponding to fibre growth steps evidenced by chemical etchings. Cyclic repartition of sulfated sugars so exactly matches the skeletal growth steps, that this correspondence strongly suggests involvement of sugars in the mineralization process. This hypothesis finds some additional support in the correlation between the biochemical diversity of these skeletal compounds and the taxonomy-linked properties of skeletal fibres, from crystallinity to isotopic fractionation.

Acknowledgments—The authors thank anonymous reviewers for helpful suggestions.

Associate editor: D. W. Lea

REFERENCES

Bar-Matthews M., Wasserburg G. J., and Chen J. H. (1993) Diagenesis of fossil coral skeletons: Correlation between trace elements, textures, and $^{234}U/^{238}U$. *Geochim. Cosmochim. Acta* **57,** 257–276.

Bryan W. B. and Hill D. (1941) Spherulitic crystallization as a mechanism of skeletal growth in the hexacorals. *Proc. Roy. Soc. Queensland* **52**(9), 78–91.

Constantz B. and Weiner S. (1988) Acidic macromolecules associated with the mineral phase of scleractinian coral skeletons. *J. Exp. Zool.* **248,** 253–258.

Cuif J. P. and Dauphin Y. (1998) Microstructural and physico-chemical characterization of "centres of calcification" in septa of some recent Scleractinian corals. *Pal. Zeit.* **72,** 257–270.

Dauphin Y. (2001) Comparative studies of skeletal soluble matrices from some Scleractinian corals and Molluscs. *Int. J. Biol. Macromol.* **28,** 293–304.

Dauphin Y. and Cuif J. P. (1997) Isoelectric properties of the soluble matrices in relation to the chemical composition of some Scleractinian skeletons. *Electrophoresis* **18,** 1180–1183.

Dauphin Y. and Cuif J. P. (1999) Relation entre les teneurs en soufre des biominéraux calcaires et leurs caractéristiques minéralogiques. *Ann. Sci. Nat.* **2,** 73–85.

Gaffey S. (1988) Water in skeletal carbonates. *J. Sedim. Petrol.* **58,** 397–414.

Gautret P., Cuif J. P., and Stolarski J. (2000) Organic components of the skeleton of scleractinian corals: Evidence from in situ acridine orange staining. *Acta Palaeont. Pol.* **45**(2), 107–118.

Gladfelter E. H. (1982) Skeletal development in *Acropora cervicornis*: I. Patterns of calcium carbonate accretion in the axial corallite. *Coral Reefs* **1,** 45–51.

Goreau T. F. (1959) The physiology of skeleton formation in corals. I. A method for measuring the rate of calcium deposition by corals under different conditions. *Biol. Bull.* **116,** 59–75.

Johnston I. S. (1980) The ultrastructure of skeletogenesis in hermatypic corals. *Int. Rev. Cytol.* **67,** 171–214.

Lowenstam H. A. (1981) Minerals formed by organisms. *Science* **211,** 1126–1131.

Mitterer R. M. (1978) Amino acid composition and metal binding capability of the skeletal proteins of corals. *Bull. Marine Sci.* **28,** 173–180.

Ogilvie M. (1896) Microscopic and systematic study of madreporarian types of corals. *R. Soc. London Phil. Trans.* **187**(B), 83–345.

Pratz E. (1882) Über die verwandschaftlichen Beziehungen einigen Korallengattungen. *Palaeontographica* **29,** 81–123.

Sorauf J. E. (1972) Skeletal microstructure and microarchitecture in Scleractinia (Coelenterata). *Palaeontology* **15**(1), 88–107.

Sorauf J. E. (1980) Biomineralization, structure and diagenesis of the coelenterate skeleton. *Acta Palaeontol. Polon.* **25,** 327–343.

Sorauf J. E. and Cuif J. P. (2001) Biomineralization and diagenesis in the Scleractinia: Part II, diagenesis. *Bull. Tohoku Univ. Museum* **1,** 152–163.